

## Research on Super Resolution Imaging Method Based on Multiple Signal Classification

Bin Zhang<sup>1</sup>, Rui Su<sup>2</sup>, Jianzu Gu<sup>1</sup>

<sup>1</sup>Faculty of Civil Engineering and Mechanics, Jiangsu University, Xuefu Road 301, Zhenjiang, Jiangsu Province, China, postal code: 212013

Corresponding Author: Jianzu Gu

<sup>2</sup>Zhengzhou University, No. 100 Science Avenue, Zhengzhou City, Henan Province, China.

Received 18 May 2020; Accepted 03 June 2020

**Abstract:** There are many ways to use ultrasound Lamb waves for damage imaging. Among them, ultrasonic phased array imaging has attracted wide attention in the field of ultrasonic imaging due to its advantages of good flexibility, high detection efficiency and high imaging accuracy. Among the existing ultrasonic phased array imaging methods, a more widely used method is an algorithm for delay superimposing time-domain signals with fixed weight values. Although this method has high imaging efficiency, it can not effectively suppress the noise of non-scanning azimuth, so side lobe artifacts will occur and the imaging resolution is not high. There are other damage detection methods such as time reversal and ellipse positioning, but these methods cannot achieve super-resolution imaging of damage because they cannot break through the Rayleigh limit. Therefore, based on the ultrasound Lamb wave phased array imaging, this paper developed a multiple signal classification algorithm. In this method, damage is detected by multiple phased arrays, and the received signal is processed by a specific algorithm to obtain super-resolution imaging. The signal is excited by M excitation elements and then received by N receiving elements. The total signal can form an  $M \times N$  matrix. After singular value decomposition of the collected signal matrix, T significant eigenvalues can be obtained, and the number of significant eigenvalues represents the number of damages. The singular vector after singular value decomposition contains the information of the noise space. Using the randomness of the noise subspace, the imaging index is formulated to restore the spatial frequency greater than  $2K$  to achieve super-resolution imaging. In this method, as long as the minimum value of M and N is greater than the number of damages, each damage can be successfully distinguished at super-resolution. Therefore, an appropriate number of matrix elements should be selected for different damage situations.

**Keywords:** nondestructive testing, ultrasonic phased array, multiple signal classification, super resolution.

### I. INTRODUCTION

Non-destructive testing technology (NDT) is a testing method that can effectively evaluate the health of the structure. It does not damage the internal structure and performance of the material when performing health testing on the structure, and can reflect the structure in real time and accurately. Internal health. Therefore, through the non-destructive testing technology to monitor the health of the structure, the reliability of the structure can be further accurately evaluated to achieve the purpose of reducing maintenance costs. In recent years, in the field of non-destructive testing, many researchers at home and abroad have done a lot of research on plate-like structures. There are many common methods in the field of nondestructive testing, and the methods worth mentioning include: X-ray method, tomography method, ultrasonic method, thermal imaging method, penetration method, etc. Among these methods, the ultrasonic method is widely used due to its limited application conditions and high imaging accuracy. In the ultrasonic method, time reversal imaging method, offset imaging method, phased array delay superimposed imaging method are the main imaging methods. Due to the limitation of Rayleigh limit<sup>[8]</sup>, super resolution cannot be achieved, that is, two Damage less than half a wavelength. Therefore, on the basis of collecting signals based on full matrix, this paper separates the signal subspace and noise subspace. The randomness of the noise space is then used to realize super-resolution imaging to resolve multiple scatterers less than half a wavelength. This article will start with the theoretical part and introduce the theoretical basis of multiple signal classification algorithm to achieve super-resolution. Then carry out numerical simulation to prove that the multiple signal classification algorithm achieves super-resolution<sup>[7]</sup> effect from the perspective of numerical simulation. Finally, relevant experiments are conducted to verify the super-resolution effect of the multiple signal classification algorithm from the experimental point of view.

## II. THE PROPOSED ENSEMBLE METHOD

Assuming that there are  $K$  damages on a board, in order to achieve full matrix acquisition, we set up a column of  $M$  sensors on the board to be used as excitation elements, and the number of each excitation element is  $x_i^a, i = 1, 2, 3, \dots, M$ ; At the same time, in order to receive the wave field information, a list of  $N$  sensors is set to be used as the receiving element for receiving the wave field information, and the number of each receiving element is  $x_j^s, j = 1, 2, 3, \dots, N$ ; For the plate and shell structure, because of its thin thickness, the damage boundary can be regarded as a two-dimensional boundary, which can be expressed by  $x^v$ . The realization of the multiple signal classification algorithm is basically based on the ultrasonic phased array for full matrix acquisition to form a covariance matrix, and then the singular value decomposition of the measured covariance matrix  $T$ . For the signal of the  $i$ -th excitation element received by the  $j$ -th reception element, we can express it as:

$$r_{ji}(x_j^s) = K_{ji}(x_j^s; x_i^a) e_i x_i^a \quad (1)$$

Among them,  $K_{ji}$  is an element in the transfer matrix  $K$ , which represents the transfer function between the  $i$ -th excitation element and the  $j$ -th reception element. Here we can regard the scattered wave field caused by damage as a secondary scattering source, so we need to define a scattering potential  $V(x)$  [1] to associate the secondary scattering source with the total wave field. From the Berne approximation, when the scattering is weak, the total wave field can be replaced by the incident wave field, so the transfer function  $K_{ji}$  can be expressed as follows:

$$K_{ji} = \int_{\partial\tau} v(x_j^s; x^v) V(x^v) u(x^v; x_i^a) dx^v \quad (2)$$

The  $u(a, b)$  and  $v(a, b)$  in this formula represents the Green's function space vector from point  $b$  to point  $a$  in the isotropic medium. When the damaged multiple sites are different from each other, that is, they are not too close to each other, the interaction between the damaged different sites is weak, so the damage imaging obtained has good resolution and can accurately distinguish each Injury [2]. However, for small lesions of individuals, it is impossible to achieve good resolution to accurately distinguish individual lesions. We can express its dispersion potential as:

$$V(x) = \sum_{k=1}^K v_k(x_k^v) \delta(x - x_k^v) \quad (3)$$

Among them,  $\delta$  represents the Kroneck symbol,  $x_k^v$  is the center of small damage,  $k = 1, 2, 3, \dots, K, (K \leq \min\{M, N\})$ ; and  $v_k$  is the surface reflectance at the center of small damage  $x_k^v$ . Therefore, equation (3) can be written as follows:

$$K_{ji} = \sum_{k=1}^K v(x_j^s; x_k^v) v_k(x_k^v) u(x_k^v; x_i^a) \quad (4)$$

Therefore, for each transfer function between the excitation element and the receiving element, a transfer matrix  $K$  can be formed, which can be written as follows:

$$K = V^s(x^s; x^v) V(x^v) U^a(x^v; x^a) \quad (5)$$

In this formula,  $x^a, x^v, x^s$  represents the position of the excitation element, the damaged position, and the position of the receiving element. The matrices  $V^s$  and  $U^a$  used to represent the space vectors of Green's function represent the matrix of Green's function space vectors from each damage to each receiving element and from each excitation element to the damage. Therefore, these two matrices can be written as follows:

$$\begin{aligned} U^a &= [u_1^a, u_2^a, \dots, u_{\min\{M, N\}}^a] \\ V^s &= [v_1^s, v_2^s, \dots, v_{\min\{M, N\}}^s] \end{aligned} \quad (6)$$

among them:

$$\begin{aligned} u_k^a &= [u(x_k^v; x_1^a), \dots, u(x_k^v; x_N^a)]^T, k = 1, 2, \dots, K \\ v_k^s &= [v(x_1^s; x_k^v), \dots, v(x_M^s; x_k^v)]^T, k = 1, 2, \dots, K \end{aligned} \quad (7)$$

The dimensions of the matrix  $V^s$  and  $U^a$  space vectors are the smallest of  $M$  and  $N$ , and the dimension is the sum of the dimensions of the noise subspace and the signal subspace. This shows that it

contains the information of the noise subspace and the signal subspace. We can write  $\| \cdot \|$  for the second norm of each vector. The superscript T indicates the transpose of the matrix.

Derived from the above, the expression of the covariance matrix can be written<sup>[3]</sup>:

$$\begin{aligned} T &= K^H K \\ T_2 &= K K^H \end{aligned} \tag{8}$$

Among them, the superscript H represents the complex conjugate transpose of the matrix. According to the proof results of Prada and Fink<sup>[4]</sup>, the singular vector  $U^a$  of the matrix  $\mathbf{u}_k^a = [u(x_k^v; x_1^a), \dots, u(x_k^v; x_N^a)]^T, k = 1, 2, \dots, K$  is one of the eigenvalues of the covariance matrix T. The expressions for T and  $T_2$  are:

$$\begin{aligned} K^H K \mathbf{u}_k^a &= |v_k|^2 \|\mathbf{u}_k^a\|^2 \|\mathbf{v}_k^s\|^2 \mathbf{u}_k^a, k = 1, 2, \dots, K \\ K^H K \mathbf{v}_k^s &= |v_k|^2 \|\mathbf{u}_k^a\|^2 \|\mathbf{v}_k^s\|^2 \mathbf{v}_k^s, k = 1, 2, \dots, K \end{aligned} \tag{9}$$

The non-zero eigenvalues of matrices T and  $T_{2T}$  are:

$$\lambda_k = |v_k|^2 \|\mathbf{u}_k^a\|^2 \|\mathbf{v}_k^s\|^2, k = 1, 2, \dots, K \tag{10}$$

Therefore, the eigenvalue decomposition of these two matrices can be simply expressed as the singular value decomposition of matrix K<sup>[5]</sup>:

$$K = \tilde{V}^s \hat{V} \tilde{U}^{aH} \tag{11}$$

Where  $\tilde{V}^s = [\tilde{\mathbf{v}}_1^s, \dots, \tilde{\mathbf{v}}_{\min\{M,N\}}^s]$  represents the left singular vector matrix and  $\tilde{U}^a = [\tilde{\mathbf{u}}_1^a, \dots, \tilde{\mathbf{u}}_{\min\{M,N\}}^a]$  represents the right singular vector matrix.  $\hat{V}$  is a diagonal matrix. Element  $\delta_k (k = 1, \dots, K)$  is a non-zero eigenvalue on the diagonal, and the eigenvector corresponding to these eigenvalues is the signal subspace. When  $k = K + 1, K + 2, \dots, \min\{M, N\}$ , the remaining eigenvalues are all zero, and the noise subspace is formed by the eigenvectors corresponding to these zero eigenvalues, and is orthogonal to the signal subspace. The relationship between the singular value decomposition of the K matrix and the eigenvalue decomposition of the two T matrices is:

$$\begin{aligned} \tilde{\mathbf{u}}_k^a &= \frac{\mathbf{u}_k^a}{\|\mathbf{u}_k^a\|}, k = 1, 2, \dots, K \\ \tilde{\mathbf{v}}_k^s &= \frac{\mathbf{v}_k^s}{\|\mathbf{v}_k^s\|}, k = 1, 2, \dots, K \end{aligned} \tag{12}$$

From the above formula, we can find that the singular vector of K is just the normalized version of the two T matrix eigenvectors, and the singular value is the square root of the corresponding eigenvalue:

$$\delta_k = |v_k| \|\mathbf{u}_k^a\| \|\mathbf{v}_k^s\|, k = 1, 2, \dots, K \tag{13}$$

The Green's function inside the background medium can be regarded as a time-scattered wave that starts from the excitation element and the reception element and propagates to any point  $x$  in the entire plate-like space and ends. The Green functions starting from the excitation element and the receiving element can be expressed as:

$$\begin{aligned} \mathbf{u}^a(x) &= [u(x; x_1^a), \dots, u(x; x_N^a)]^T \\ \mathbf{v}^s(x) &= [v(x; x_1^s), \dots, v(x; x_M^s)]^T \end{aligned} \tag{14}$$

According to the orthogonal characteristics of the feature vector<sup>[6]</sup>:

$$\begin{aligned} \tilde{\mathbf{u}}_k^a \cdot \mathbf{u}^a(x) &= \begin{cases} \|\mathbf{u}_k^a\| & x = x_k \\ 0 & x \neq x_k \end{cases} k = 1, \dots, K \\ \tilde{\mathbf{v}}_k^s \cdot \mathbf{v}^s(x) &= \begin{cases} \|\mathbf{v}_k^s\| & x = x_k \\ 0 & x \neq x_k \end{cases} k = 1, \dots, K \end{aligned} \tag{15}$$

From the derivation of formula (15), we can separately formulate imaging indexes for the Lamb wave propagating from the excitation element to the damage and the Lamb wave propagating from the damage to the receiver:

$$I^a(x) = \frac{1}{\min\{M,N\} \sum_{k=K+1} \tilde{\mathbf{u}}_k^a \cdot \mathbf{u}^a(x)}$$

$$I^s(x) = \frac{1}{\min\{M,N\} \sum_{k=K+1} \tilde{\mathbf{v}}_k^s \cdot \mathbf{v}^s(x)}$$
(16)

Then the two sets of imaging indexes are combined to obtain the imaging index that can ultimately achieve super resolution:

$$I(x) = \frac{1}{\sum_{k_1=K+1} \tilde{\mathbf{u}}_{k_1}^a \cdot \mathbf{u}^a(x) \sum_{k_2=K+1} \tilde{\mathbf{v}}_{k_2}^s \cdot \mathbf{v}^s(x)}$$
(17)

### III. NUMERICAL SIMULATION

In the numerical simulation part, in order to verify the accuracy of the algorithm for damage localization and the super-resolution effect of imaging, isotropic material plates with preset single damage and preset double damage were prepared respectively, and the aluminum plate was selected here. The geometric size of the aluminum plate is 460mm × 300mm × 1mm, the geometric size of the piezoelectric sensor is 4mm × 4mm × 1mm, the position of the PZT1 is used as the origin, and the 16 PZTs are arranged as a uniform linear array with a center spacing of 5mm. Among them, the piezoelectric chips PZT1 and PZT9 are the excitation sources, and the single excitation is sequentially performed, and PZT1 ~ 16 are used as the receiving element to receive the wave field signal of each excitation. In the single-damage model, the damage is a hole with a diameter of d = 3mm, the left side of the damage is 207mm from the left side of the plate, and the distance from the top of the plate is 67mm. The specific distribution diagram is shown in Figure 1 (a). In the double-damage model, it is necessary to consider that the distance between the two damages must satisfy d < λ / 2, that is, less than half of the carrier. The center frequency of the excitation signal used here is 150KHz, and the wavelength can be calculated from the dispersion curve to be 9.87mm, so the distance between the two damages is set to 4.5mm. The specific model diagram is shown in Figure 1 (b).

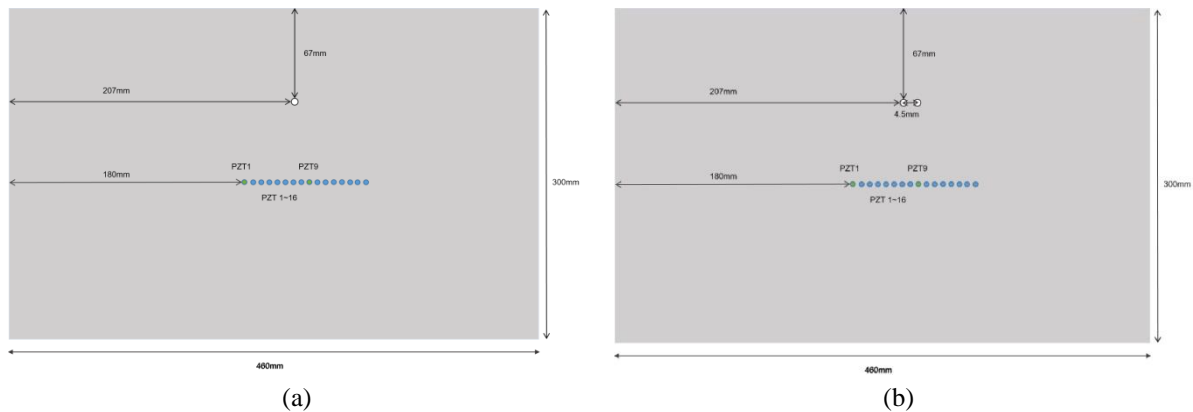


**Figure 1:** (a)Single damage model diagram;(b)Double damage model diagram;

#### 1.Single damage imaging

The excitation signals are sent out at the positions of PZT1 and PZT9 respectively, and then the response signals are received at the various collection points set on the board. For the received response signal, the window function is used to extract the scattered wave signal. For the extracted scattered wave signals, the phased array delay superimposed beamforming algorithm (DAS) and the multiple signal classification algorithm (MUSIC) are used, respectively, and the resulting injury imaging 2D and 3D images are shown in Figures 2 and 3, respectively. The left side is the traditional delayed superimposed beamforming algorithm (DAS) imaging map, and the right side is the multiple signal classification algorithm (MUSIC) imaging map. The unit of length in the figure is meter (m), and the circle is the location of single damage. The shape of the damage in this

simulation is a hole with a radius of 3 mm, and the preset position is (0,110). The damage position calculated by the final imaging map obtained by the DAS algorithm is (-3,116), which deviates from the true damage center by 6.71mm, the relative error of the damage center distance is 8.39%, and the imaged area is increased by 134.93% compared to the actual damage area. In general, the damage location can only be achieved in general. While using the MUSIC algorithm to locate the damage, the location of the damage is (-1,112), which is only 2.23mm away, and the relative error is only 2.75%, which achieves the accurate positioning of the damage. The imaging area is only 5.72% larger than the real area. From the simulation imaging results of single damage, this method can accurately locate the location of the damage, and it is very possible to achieve super-resolution. Whether super resolution can be achieved in the end depends on whether the algorithm can finally distinguish two damages less than half a wavelength.

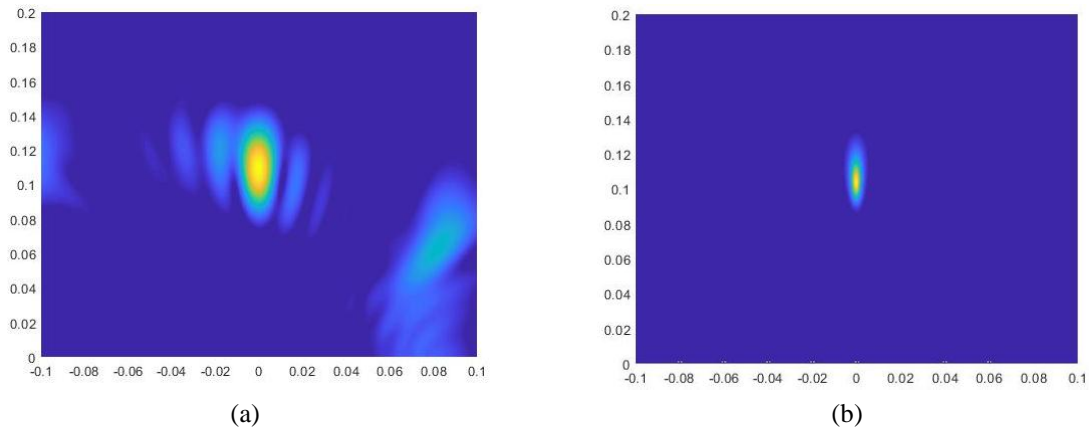


**Figure 2** 2D single damage imaging: (a)delay and sum beamforming;(b)multiple signal classification.

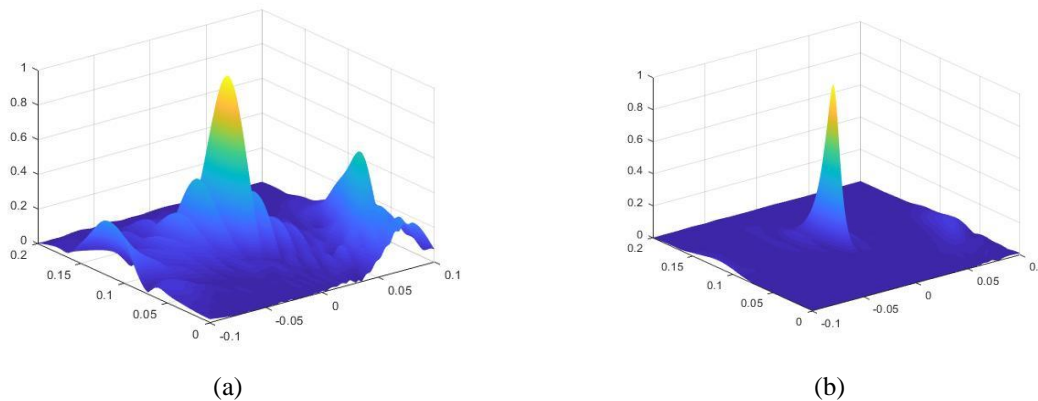


**Figure 3** 3D single damage imaging: (a)delay and sum beamforming;(b)multiple signal classification.

### 2.Double damage imaging

For the double-damage model, because the two excitation elements are sequentially excited, it needs to be processed according to the following methods: No. 1 piezoelectric plate is excited, and the position of the No. 1 piezoelectric plate receives the signal; Position excitation, 1 ~ 16 piezoelectric piece position receiving signal. The damage scattered wave signal is extracted through the window function. For the extracted damage scattered wave signals, the dual-damage imaging map as shown in Fig. 4 is obtained by the delayed superimposed beamforming algorithm (DAS) and the multiple signal classification algorithm (MUSIC), respectively.

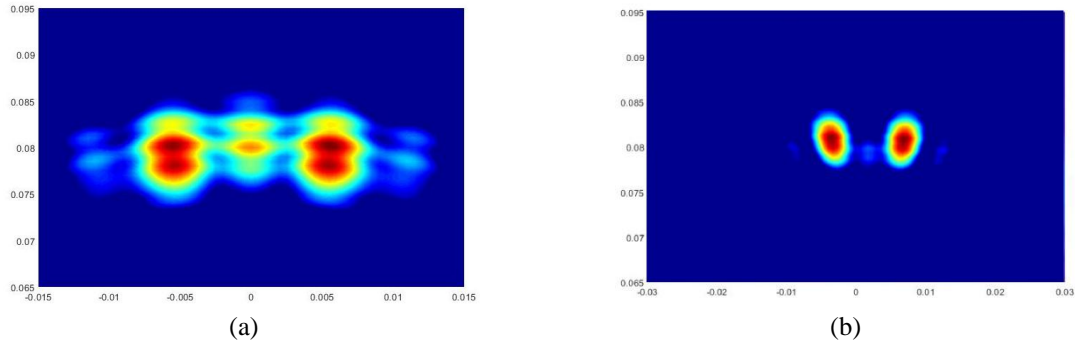


**Figure 4** Double damage imaging: (a)delay and sum beamforming;(b)multiple signal classification.

Based on the imaging results obtained, the damage location and various error results can be calculated. It can be seen from the calculation results that the MUSIC algorithm not only locates the specific locations of the two damages more accurately than the DAS algorithm. More importantly, in the face of two damages with a distance of 4.5mm smaller than the half-wavelength of the carrier, DAS cannot clearly distinguish the two damages, but the MUSIC algorithm successfully distinguishes the two damages. Combined with the imaging results of single damage, it is fully demonstrated that the MUSIC algorithm can not only achieve accurate positioning of the damage, but also resolve multiple damage with a spacing of less than half a wavelength, and achieve super-resolution imaging of the damage.

#### IV. EXAMPLE PROBLEMS

The PZT-SLDV hybrid detection system is used in this experiment. Taking the center position of the aluminum plate as the coordinate origin 1mm as the unit length, PZT as the excitation element located at (-10,0), (0,0) and (10,0) to send the excitation signal, the scanning points of SLDV form a linear Array to collect wave field information. The linear array composed of scanning points is evenly distributed along the x-axis. The interval between each scanning point is 0.5mm.  $-100\text{mm} \leq x \leq 100\text{mm}$  is the scanning interval. The sampling frequency is 5.12MHz, the time step is  $\Delta t = 1.95 \times 10^{-7}$  s, and the total time is  $200\mu\text{s}$ . For the response signals of each scanning point collected by SLDV, the damage scattered wave obtained after removing the direct wave and the boundary reflected wave is eliminated. The damage imaging can be obtained by using the damage scattered waves through the DAS algorithm and the MUSIC algorithm respectively.

##### 1. Single damage imaging

In the experiment, the response signal collected for the pre-set single-damaged aluminum plate was removed the direct wave and the boundary reflection wave to obtain the damage scattering signal. Then, imaging methods consistent with numerical simulation are used, and damage scattering signals are used for damage imaging. The resulting damage imaging results are shown in Figure 5. Among them (a) is the damage imaging map obtained by the delayed superimposed beamforming algorithm (DAS), and (b) is the damage imaging map obtained by the multiple signal classification algorithm (DAS).

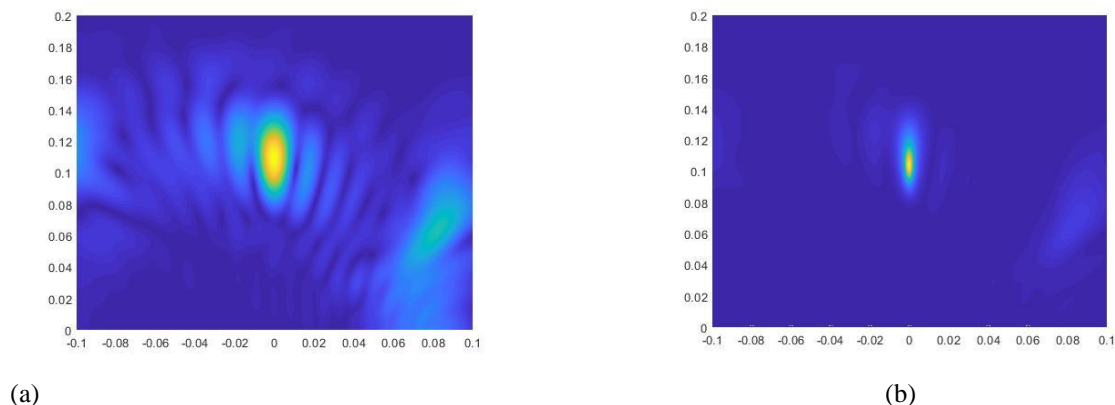


**Figure 5** Single damage imaging: (a)delay and sum beamforming;(b)multiple signal classification.

As can be seen from Figure 5, due to the influence of noise, in the damage imaging map obtained by the DAS algorithm, the size of the damage imaging area is much larger than the true size of the damage, and there are multiple false peak spectra near the damage location. To judge the damage. In the damage imaging map obtained by the MUSIC algorithm, the size of the damage imaging area is closer to the true size of the damage, and no false peak spectrum appears near the damage location, showing a more reliable damage localization effect. . By calculating the various errors, it can be known that the MUSIC algorithm achieves more accurate damage location and more accurate determination of the shape of the damage than the traditional DAS algorithm. Although some noise exists during the experiment, due to the non-strong correlation noise and the reasonable array element spacing setting, it does not have much impact on the imaging result of the MUSIC algorithm, so the MUSIC algorithm exhibits in the presence of noise More reliable damage location effect. Combined with the experimental results, it can still be seen that the MUSIC algorithm can achieve precise positioning of damage, and has the potential to achieve super-resolution. In the next step, the MUSIC double-damage imaging experiment results can be used to judge whether the MUSIC algorithm can achieve super-resolution damage imaging.

## 2.Double damage imaging

For the damage scattered waves extracted in the double-damage experiment, the imaging methods consistent with the numerical simulation were used to perform the imaging of the damage, respectively, and the resulting imaging results of the damage are shown in FIG. Among them (a) is the damage imaging map obtained by the delayed superimposed beamforming algorithm (DAS), and (b) is the damage imaging map obtained by the multiple signal classification algorithm (DAS).

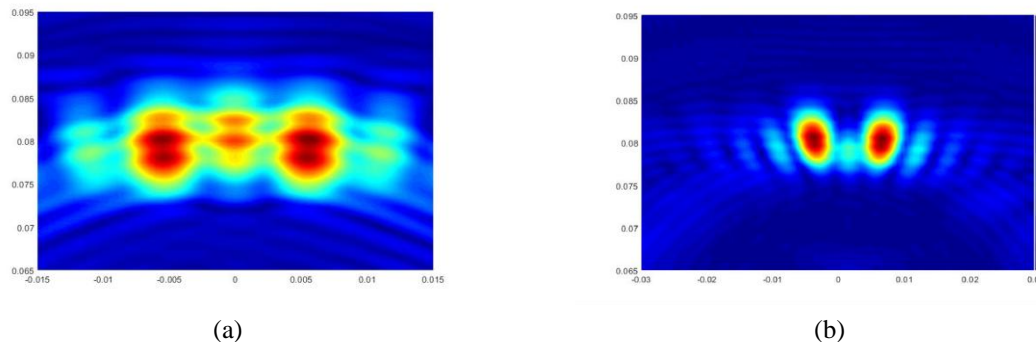


**Figure 6** Double damage imaging: (a)delay and sum beamforming;(b)multiple signal classification.

According to the calculation of various errors from the imaging map, it can be seen that the DAS algorithm cannot distinguish the two damages less than half the wavelength, and the MUSIC algorithm successfully distinguishes the two damages less than half the wavelength and successfully locates the damage position. The experimental results prove that the MUSIC algorithm can successfully achieve super-resolution damage imaging.

## V. CONCLUSION

From a theoretical point of view, the multiple signal classification algorithm (MUSIC) separates the signal subspace and the noise subspace. By using the randomness of the noise subspace, the super-resolution effect is achieved in the final imaging result. According to the results of experiments and simulations, it is also verified that the MUSIC algorithm can not only achieve accurate positioning of damage, but also distinguish two damages less than half a wavelength, and achieve super-resolution damage imaging effect.

## REFERENCES

- [1]. Devaney, Anthony J. Mathematical Foundations of Imaging, Tomography and Wavefield Inversion[J]. 2012.
- [2]. Gruber F, Marengo E and Devaney A. Time-reversal imaging with multiple signal classification considering multiple scattering, between the targets[J]. Acoust Soc Am 2004; 115(6): 3042–3047.
- [3]. Fink, M. Time reversal of ultrasonic fields. I. Basic principles[J]. IEEE Transactions on Ultrasonics Ferroelectrics & Frequency Control, 1992, 39(5):0-566.
- [4]. Prada C , Fink M . Eigenmodes of the time reversal operator: A solution to selective focusing in multiple-target media[J]. Wave Motion, 1994, 20(2):151-163.
- [5]. Lehman S K , Devaney A J . Transmission mode time-reversal super-resolution imaging[J]. The Journal of the Acoustical Society of America, 2003, 113(5):2742-2753.

## ***Research on Super Resolution Imaging Method Based on Multiple Signal Classification***

---

- [6]. Gruber F K , Marengo E A , Devaney A J . Time-reversal imaging with multiple signal classification considering multiple scattering between the targets[J]. Journal of the Acoustical Society of America, 2004, 115(6):3042-3047.
- [7]. Chen F C , Chew W C . Experimental verification of super resolution in nonlinear inverse scattering[J]. Applied Physics Letters, 1998, 72(23):3080.
- [8]. Lehman SK and Devaney AJ. Transmission mode time reversal super-resolution imaging. J Acoust Soc Am 2003;113(5): 2742-2753.

Bin Zhang, et. al. "Research on Super Resolution Imaging Method Based on Multiple Signal Classification." *IOSR Journal of Engineering (IOSRJEN)*, 10(5), 2020, pp. 39-46.